Origin of chaos in soft interactions and signatures of nonergodicity

M. W. Beims,[1,2] C. Manchein,[1] and J. M. Rost[2]
[1]*Departamento de Física, Universidade Federal do Paraná, 81531-990 Curitiba, PR, Brazil*
[2]*Max Planck Institute for the Physics of Complex Systems, Nöthnitzer Strasse 38, D-01187 Dresden, Germany*
(Received 13 February 2006; revised manuscript received 5 August 2007; published 2 November 2007)

The emergence of chaotic motion is discussed for hard-point like and soft collisions between two particles in a one-dimensional box. It is known that ergodicity may be obtained in hard-point like collisions for specific mass ratios $\gamma=m_2/m_1$ of the two particles and that Lyapunov exponents are zero. However, if a Yukawa interaction between the particles is introduced, we show analytically that positive Lyapunov exponents are generated due to double collisions close to the walls. While the largest finite-time Lyapunov exponent changes smoothly with γ, the number of occurrences of the most probable one, extracted from the distribution of finite-time Lyapunov exponents over initial conditions, reveals details about the phase-space dynamics. In particular, the influence of the integrable and pseudointegrable dynamics without Yukawa interaction for specific mass ratios can be clearly identified and demonstrates the sensitivity of the finite-time Lyapunov exponents as a phase-space probe. Being not restricted to two-dimensional problems such as Poincaré sections, the number of occurrences of the most probable Lyapunov exponents suggests itself as a suitable tool to characterize phase-space dynamics in higher dimensions. This is shown for the problem of two interacting particles in a circular billiard.

DOI: 10.1103/PhysRevE.76.056203 PACS number(s): 05.45.Ac

I. INTRODUCTION

The investigation of the origin of chaotic motion in standard billiard models (such as the Sinai billiard [1], the Bunimovich stadium [2], or the Annular billiard [3]), has played a pioneering role since the very beginning of chaos theory. Usually, in such models, ballistic chaotic motion (single-particle dynamics) is a consequence of the spatial billiard geometry. For interacting many-particles systems, which appear in many areas of physics, chaotic motion can be generated from the combined effect of external forces and mutual interactions. In order to understand how chaotic motion emerges as a consequence of the interaction between particles, a simple billiard—namely, a one-dimensional (1D) box—will be used. Since in this case the boundary alone cannot induce irregular motion of the two particles inside, the role of the interaction for the generation of chaotic motion becomes clear.

Interacting particles inside billiards can be used to model electrons in quantum dots. Electrons are confined inside a disk and are affected by the surrounding material which composes the semiconductor [4]. In fact, the composition of the surrounding material may destroy the long Coulomb repulsion between electrons and also change the effective mass between particles [5]. The influence of both effects on quantum energy levels and/or electrons dynamics is not obvious. However, they can be studied in detail for a physical model where the kinetic and potential energy of the particles can be varied independently. This is achieved by a parameter which controls the range of interaction between the particles (electrons) and by varying the mass ratio $\gamma=m_2/m_1$ of the particles.

In this paper we will study the classical dynamics of two interacting particles inside a one-dimensional billiard as a function of γ and as a function of the interaction range between particles. A Yukawa interaction between particles is assumed. Such a system has been considered classically [6] and quantum mechanically [7] for the case of equal masses. In order to calculate the spectrum of Lyapunov exponents (LEs), the dynamics in tangent space is determined explicitly. In the limit of a very short range of interaction, this system should approach the hard-point collision case analyzed originally by Casati and Ford [8]. Despite ergodic dynamics for the case of pointlike collisions at specific γ, vanishing LEs are a consequence of the linear instability of this system [9]. Such linear-unstable systems have become a topical problem in statistical mechanics [10] (see also about the origin of diffusion in nonchaotic systems [11]).

In the case of a Yukawa interaction, the repulsion between particles *at collisions with the walls* are shown to generate positive LEs. This is shown explicitly by determining the dynamics in tangent space. While the mean value of the largest finite-time LE only quantifies the degree of chaoticity of the system, the number of occurrences of the most probable LE, extracted from the distribution over initial conditions, is shown to give significant information about regular structures and sticky (or trapped) [12] trajectories in phase space. This distribution is determined numerically as a function of γ.

The plan of the paper is as follows. Section II reviews the main results from the problem of two hard-point particles in a one-dimensional box. In Sec. III chaotic motion emerges with the introduction of the soft Yukawa interaction between the particles. Positive LEs can be generated from analytical expressions obtained for the dynamics in tangent space. The distribution of the largest finite-time LE calculated over the phase space of initial conditions is used to reveal the underlying dynamics. Section III discusses the distribution of the largest finite-time LE for the case of two interacting particles in a circular billiard. The paper ends with conclusions in Sec. V.

II. TWO PARTICLES IN A 1D BOX WITH HARD-POINT-LIKE COLLISIONS

Two particles in a 1D box with hard-point like collisions, also called two-particle hard-point gas, can also be treated as a particular case of the motion of three particles on a finite ring [13,14], which can be mapped onto the motion of a particle in a triangle billiard [15]. In such systems the Lyapunov exponent is zero [9] and the whole dynamics can be monitored by changing the angles of the triangle billiard. These angles are functions of the masses ratio between particles. Such triangle billiards have also been applied to study energy diffusion in one-dimensional systems [9]. Although the connection to the triangle billiard is very useful to gain insights into the collision properties of the particles, it is not needed for the purpose of the present work.

As follows, we summarize the main results obtained by Casati and Ford [8], which are similar to those observed in the triangle billiard. Using Poincaré sections they [8] showed that the dynamics is nonergodic if θ is a rational multiple of π, where

$$\cos(\theta) = \frac{1 - m_2/m_1}{1 + m_2/m_1} = \frac{1-\gamma}{1+\gamma} = \Delta. \tag{1}$$

More specifically, writing $\theta = \frac{m}{n}\pi$, where m and n are integers, at most $4n$ distinct velocity values occur. On the other hand, when θ is an irrational multiple of π, the velocities become uniformly dense [16] in velocity space. As a consequence, it is at least *possible* for the two-particle hard-point gas to be ergodic in velocity space if θ/π is irrational. Although Casati and Ford [8] did not show explicit results for irrational multiples of π, they argued that their numerical results provide evidence supporting ergodic behavior for irrational θ/π by demonstrating that an increasing number of velocities is observed for a sequence of rational θ/π approaching an irrational θ/π value. Note, however, that for irrational θ/π infinite time may be required to observe all velocities.

Although there are infinitely many mass ratios which give rational values of θ/π, some of them are special. First, the integrable cases [17] $\gamma = 1, 3$ (or 1/3), which have $\theta = \frac{1}{2}\pi$ and $\theta = \frac{2}{3}\pi$ (or $\pi/3$), respectively. Relating Eq. (1) with results for the triangle billiard [18] (or even to the polygonal billiard [19–21]), it is possible to show that for the integrable cases the genus is equal, $g=1$ (the invariant surface of the billiard flow is a torus). For all other rational θ/π the dynamics is pseudointegrable [14] and the invariant flow is not a torus ($1 \le g < \infty$). For genus $g=2$, the possible values of θ are [18] $\frac{1}{5}\pi, \frac{2}{5}\pi$ and the mass ratios are $\gamma \sim 0.1$ and $\gamma \sim 1.9$, respectively. As the genus increases, the invariant surface gets more and more complicated. Therefore, besides the integrable cases, the third special case, which has a "simpler" invariant surface, is expected for the pseudointegrable case $\gamma \sim 1.9$ (we do not use $\gamma \sim 0.1$ because we are interested in values of γ in the interval [1,4]). Later we will come back to the special values $\gamma = 1.0, 1.9, 3.0$.

The momentum distribution looks quite different for irrational mass ratios. Although the motion can be ergodic, the number of momenta increases *very* slowly with longer system evolution [22]. However, this aspect is not in our present focus.

III. TWO PARTICLES IN A 1D BOX WITH YUKAWA INTERACTION

It is adequate to introduce the center-of-mass and relative coordinates

$$R = \frac{m_1 q_1 + m_2 q_2}{M} \quad \text{and} \quad r = q_1 - q_2, \tag{2}$$

respectively, with the total mass $M = m_1 + m_2$ and the reduced mass $\mu = m_1 m_2/(m_1+m_2)$. In these new coordinates, the equations of motion describe a single composite particle in the hyperspace (r,R), called a hyperbilliard [7]. The Hamiltonian in relative coordinates is given by

$$H = \frac{P^2}{2M} + \frac{p^2}{2\mu} + V_0 \frac{e^{-\alpha r}}{r} = E, \tag{3}$$

where the Yukawa potential $V(r)$ has strength V_0 and the parameter $\alpha \ge 0$ gives the interaction range $r_0 = 1/\alpha$. Using scaled coordinates defined by $(\alpha \neq 0)$

$$r = r_0 \tilde{r}, \quad p = \tilde{p}\sqrt{E}, \quad R = r_0 \tilde{R},$$

$$P = \tilde{P}\sqrt{E}, \quad dt = \frac{r_0}{\sqrt{E}} d\tau,$$

and dividing Eq. (3) by E, the scaled new Hamiltonian is

$$\tilde{H} = \frac{\tilde{P}^2}{2M} + \frac{\tilde{p}^2}{2\mu} + \tilde{V}(\tilde{r}) = \epsilon = 1, \tag{4}$$

with

$$\tilde{V}(\tilde{r}) = \tilde{V}_0 \frac{e^{-\tilde{r}}}{\tilde{r}}, \quad \tilde{V}_0 = \frac{V_0}{r_0 E}, \tag{5}$$

and scaled energy $\epsilon = 1$. When $\alpha = 0$ $(r_0 \to \infty)$ the transformation is independent of r_0 and $\tilde{V}_0 = \frac{V_0}{E}$. Under $\tilde{V}(\tilde{r})$ the composite's particle relative motion is subject to the force $\tilde{Q}(\tilde{r}) = -\partial \tilde{V}/\partial \tilde{r}$ while its center-of-mass motion in $\tilde{R}$ is free. For the case of equal masses the chaotic motion of (3) was already analyzed [6].

A. Dynamics in tangent space, Lyapunov exponents, and the origin of chaotic motion

This section is dedicated to the analytical calculation of the Lyapunov spectrum. LEs are very useful to describe the dynamics in complex systems [23]. When the motion is chaotic, at least one LE is positive. Its value is determined through the dynamics in tangent space, as will be shown below.

Between collisions with the walls, the equations of motion have the form

$$\tilde{F}(\tilde{\gamma}) = (\dot{\tilde{r}}, \dot{\tilde{R}}, \dot{\tilde{v}}, \dot{\tilde{V}})^t = (\tilde{v}, \tilde{V}, \tilde{Q}(r), 0)^t, \tag{6}$$

and it is easy to see that center-of-mass momentum $M\dot{\tilde{R}}$ is a constant of motion. In relative coordinates, the composite particle moves under the influence of the force $\tilde{Q}(\tilde{r})$. This is a one-dimensional motion, which is regular and integrable. Collisions with left and right walls cause a breaking of the translational symmetry of the system, and as a consequence, the center-of-mass momentum is not a constant of motion anymore. The effect of left (right) wall collisions lead to the following change in the phase-space point $\tilde{\gamma}_i = (\tilde{r}^i, \tilde{R}^i, \tilde{v}^i, \tilde{V}^i)$ before the collision to $\tilde{\gamma}_f = (\tilde{r}^f, \tilde{R}^f, \tilde{v}^f, \tilde{V}^f)$ after the collision $\tilde{\gamma}_f = \tilde{\mathbf{D}}_k \tilde{\gamma}_i$, with

$$\tilde{\mathbf{D}}_k = (-1)^k \begin{pmatrix} 1 & 0 & 0 & 0 \\ 0 & 1 & 0 & 0 \\ 0 & 0 & -\Delta & 2 \\ 0 & 0 & 2\frac{\mu}{M} & \Delta \end{pmatrix}, \tag{7}$$

where $\Delta = (m_1 - m_2)/M$. The label $k = 1(2)$ is used for particle 1(2). Since the two particles can never pass each other in the one-dimensional billiard, it is assumed without loss of generality that particle 1(2) never collides with the right (left) wall. The complete time evolution in phase space can be formulated by integrating the equation of motion between collisions with the walls and by taking into account $\tilde{\gamma}_f$ from Eq. (7) each time the composite particle collides with the walls.

In order to calculate Lyapunov exponents, the time evolution of an infinitesimal path difference (the nearby trajectory) in the scaled tangent space ($\delta\tilde{\gamma}$) must be determined, given by

$$\delta\tilde{\gamma}(\tau) = \tilde{\mathbf{M}}(\tau)\, \delta\tilde{\gamma}(\tau_0), \tag{8}$$

with the scaled monodromy matrix

$$\tilde{\mathbf{M}}(\tau) = \frac{d\tilde{\gamma}(\tau)}{d\tilde{\gamma}(\tau_0)}. \tag{9}$$

Lyapunov exponents are the average rates of growth or shrinkage of such infinitesimal changes that are the eigenvectors of $\tilde{\mathbf{M}}$,

$$\tilde{\lambda}_i = \lim_{\tau \to \infty} \frac{\ln \tilde{\mu}_i(\tau)}{\tau}, \tag{10}$$

where $\tilde{\mu}_i(\tau)$ is the ith eigenvalue of $\tilde{\mathbf{M}}$. The matrix $\tilde{\mathbf{M}}$ can be written itself as a product of matrices for small time steps. Since the motion between collisions is regular, the Lyapunov exponents are zero. The situation is different for collisions of the composite particle with the walls. We follow the algorithm developed by Dellago *et al.* [24] to formulate the equations in the scaled tangent space according to

$$\delta\tilde{\gamma}_f = \frac{\partial \tilde{C}}{\partial \tilde{\gamma}_i} \delta\tilde{\gamma}_i + \left[\frac{\partial \tilde{C}}{\partial \tilde{\gamma}_i} \tilde{F}(\tilde{\gamma}_i) - \tilde{F}(\tilde{C}(\tilde{\gamma}_i)) \right] \delta\tau_f, \tag{11}$$

where $\tilde{C} = \tilde{\mathbf{D}}_k \tilde{\gamma}_i$ gives the transformation at collisions with the walls with $\tilde{\mathbf{D}}_k$ from Eq. (7). $\delta\tau_f$ is the delay in the collision time of the (infinitesimal) nearby trajectory with respect to the collision time of the reference trajectory. Between the collision time of the main trajectory and the collision time of the nearby trajectory, the composite particle moves under the influence of the force $\tilde{Q}(r)$ and the delay time can be determined from

$$t_k = \frac{\partial S_k}{\partial E} = m_k \int_{q_k^0}^{q_k^n} \frac{\partial \dot{q}_k}{\partial E} dq_k = \int_{q_k^0}^{q_k^n} \frac{dq_k}{\dot{q}_k}, \tag{12}$$

where S_k is the action of the k particle, q_k^0 is the position of the nearby trajectory when the main trajectory collides with the wall, and q_k^n is the collision point of the nearby trajectory. The energy dependence for $\dot{q}_k$, $\dot{q}_1 = \sqrt{2m_1\left(E - \frac{1}{2}m_2\dot{q}_2^2 - V_0\frac{e^{-\alpha r}}{r}\right)}$, is obtained from the energy conservation. Using Eqs. (2) we have

$$q_{1(2)} = R - \frac{(-)^{1(2)} m_{2(1)}}{M} r, \tag{13}$$

$$\dot{q}_{1(2)} = V - \frac{(-)^{1(2)} m_{2(1)}}{M} v, \tag{14}$$

and Eq. (12) can be written as

$$t_k = \int_{R_0}^{R_n} \frac{M dR}{MV - (-)^{1(2)} m_{2(1)} v} - (-)^{1(2)} \int_{r_0}^{r_n} \frac{m_{2(1)} dr}{MV - (-)^{1(2)} m_{2(1)} v}. \tag{15}$$

Since V and v does not depend on R, the integral in R can be determined analytically. After the integration of Eq. (15), terms proportional to $\delta R^i = R_0 - R_n$ and $\delta r^i = r_0 - r_n$ will appear [quadratic terms $(\delta R)^2$ and $(\delta r^i)^2$ can be neglected in the linear analysis] and it can be written in scaled relative coordinates as

$$-\delta\tau_f = \tilde{t}_k = \frac{t}{\sqrt{E}} = \tilde{A}_k \delta\tilde{R}^i + \tilde{B}_k \delta\tilde{r}^i, \tag{16}$$

where

$$\tilde{A}_{1(2)} = \frac{M}{M\tilde{V}^i - (-)^{1(2)} m_{2(1)} \tilde{v}^i},$$

$$\tilde{B}_{1(2)} = \frac{-(-)^{1(2)}}{\delta\tilde{r}^i} \int_{\tilde{r}_0}^{\tilde{r}_n} \frac{m_{2(1)} d\tilde{r}}{M\tilde{V} - (-)^{1(2)} m_{2(1)} \tilde{v}}.$$

Finally, using Eqs. (6), (7), and (16), in (11), the collision of the composite particle in tangent space with left ($k=1$) and right walls ($k=2$) under a force $\tilde{Q}(\tilde{r}) = -\partial\tilde{V}/\partial\tilde{r}$ takes the form $\delta\tilde{\gamma}_f = \tilde{\mathbf{M}}_k \delta\tilde{\gamma}_i$ with

$$\tilde{\mathbf{M}}_k = (-)^k \begin{pmatrix} -\Delta & 2 & 0 & 0 \\ 2\frac{\mu}{M} & \Delta & 0 & 0 \\ -\Delta_k \tilde{Q}\tilde{B}_k & -\Delta_k \tilde{Q}\tilde{A}_k & -\Delta & 2 \\ -2\frac{\mu}{M}\tilde{Q}\tilde{B}_k & -2\frac{\mu}{M}\tilde{Q}\tilde{A}_k & 2\frac{\mu}{M} & \Delta, \end{pmatrix}, \quad (17)$$

where $\Delta_k = -[\Delta + (-1)^k]$. The determinant of $\tilde{\mathbf{M}}_k$ is equal to 1 and eigenvalues are also equal to $|1|$. However, the matrix elements proportional to Δ_k, $\tilde{Q}$, $\tilde{A}_k$, and $\tilde{B}_k$ generate positive LEs when the global monodromy matrix $\tilde{\mathbf{M}}$ is constructed. Therefore, the presence of the interaction force $\tilde{Q}$ and terms $\tilde{A}_k$ and $\tilde{B}_k$, related to the time delay in the tangent-space collision dynamics, are essential for the chaotic properties of the system. Otherwise, if $\tilde{Q}=0$, no positive LE can be obtained.

Two limiting situations can be discussed. (a) The long-range interaction ($\alpha=0.0$, $r_0 \to \infty$): at each collision with the wall, the interaction force $\tilde{Q}(r)$ is finite and positive LEs are generated. (b) The short-range interaction ($r_0 \ll 1$): in general $\tilde{Q}(r)$ is close to zero if particles are sufficiently separated and the LEs are zero. However, the dynamics becomes chaotic due to a *double-collision* process—for example, assuming that particles 1 and 2 are moving close together toward the left wall with a mutual repulsion close to zero due to the short-range nature of the interaction. As particle 1 collides with the left wall, it changes its direction and moves toward particle 2, interacting with it. If such a double collision occurs infinitely close to the wall, the terms $\tilde{Q}\tilde{B}_k$ and $\tilde{Q}\tilde{A}_k$ are not necessarily zero, a positive LE is generated, and chaotic motion appears. This crucial role of double collisions to generate chaotic motion was also observed in another model of two interacting particles [22]. The chaotic motion induced by the soft potential will be discussed in more detail in the next section.

B. Signatures of regular motion in the distribution of largest finite-time Lyapunov exponents

From the description of the dynamics by the monodromy matrices as constructed in the last section, it is clear that chaotic dynamics is generated in the presence of a soft interaction potential. The interesting question, however, is if any signatures of nonergodicity from the hard-point collision, or stickiness, can be identified. To this end we have investigated the distribution $P(\Lambda_t, \gamma)$ of the finite-time largest Lyapunov exponents [25] Λ_t as a function of the mass ratio γ. In general, for infinite time, the LEs Λ_∞ are well defined and do not depend on initial conditions. This holds also true for reasonably large finite times if the motion is ergodic and the Lyapunov spectrum has good convergence properties. In quasiregular systems, however, where the chaotic trajectory may approach a regular island and can be trapped there for a while, the value of the local LE can decrease. This will affect the convergence of Λ_t, which depends now on the initial conditions. On the other hand, it implies that the distribution $P(\Lambda_t)$, calculated over many initial conditions, contains information about the amount of regular motion (and sticky trajectories) in phase space. Usually, for fully chaotic systems $P(\Lambda_t, \gamma)$ has a Gaussian distribution (see, for example, [26] and references therein).

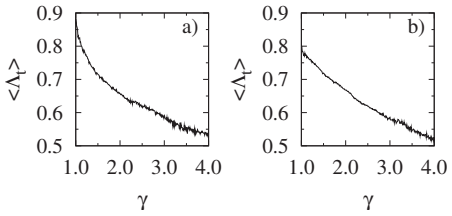

FIG. 1. Mean value of the finite-time largest Lyapunov exponent calculated over 400 trajectories up to time $t=10^4$ and at scaled energy $\epsilon=1$, for (a) long interaction range ($r_0 \to \infty$)—i.e., $\tilde{V}_0=0.1$—and (b) short-range interaction ($r_0=0.1$)—i.e., $\tilde{V}_0=1.0$—with the hard walls located at $q=\pm 1$. For each trajectory the largest LE is evaluated over 10^5 initial conditions.

The mean $\langle \Lambda_t \rangle$, shown in Figs. 1(a) and 1(b), decreases monotonically from roughly 0.9 to 0.54 in Fig. 1(a) ($r_0 \to \infty$) and from 0.80 to 0.53 in Fig. 1(b) ($r_0=0.1$) over a change of γ from 1.0 to 4.0. This means that the dynamics is getting more and more regular as expected since $\gamma \to \infty$ constitutes an integrable limit with the heavy particle at rest. Figure 2 shows the finite-time distribution of the largest LE, $P(\Lambda_t, \gamma)$, for the case of long-range interaction ($r_0 \to \infty$). It reveals two indications for increasingly regular motion with growing mass ratio: (a) the *value* of $\langle \Lambda_t(\gamma) \rangle$ itself decreases and (b) an increasing number of initial conditions lead to $\Lambda_t(\gamma)$ close to zero (related to sticky trajectories) or converge exactly to zero (regular islands). At $\gamma=4.0$, for example, about 15% of the initial conditions lead to $\Lambda_t=0$. The gray points below the main curve are related to chaotic trajectories which were trapped for a while close to regular islands. Some examples will be given below. An interesting feature in Fig. 2 is the change of the width of $P(\Lambda_t, \gamma)$ around the most probable Λ_t^p defined through

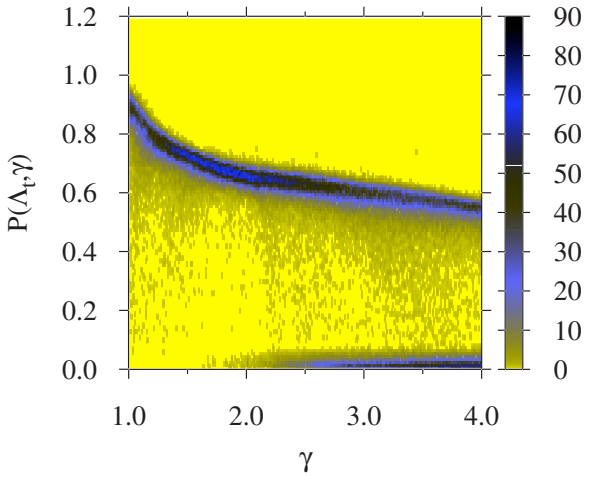

FIG. 2. (Color online) Finite-time distribution of the largest Lyapunov exponent $P(\Lambda_t, \gamma)$ calculated over 400 trajectories up to time $t=10^4$ and for $r_0 \to \infty$. With increasing $P(\Lambda_t, \gamma)$ the color changes from light to dark (white over yellow and blue to black).

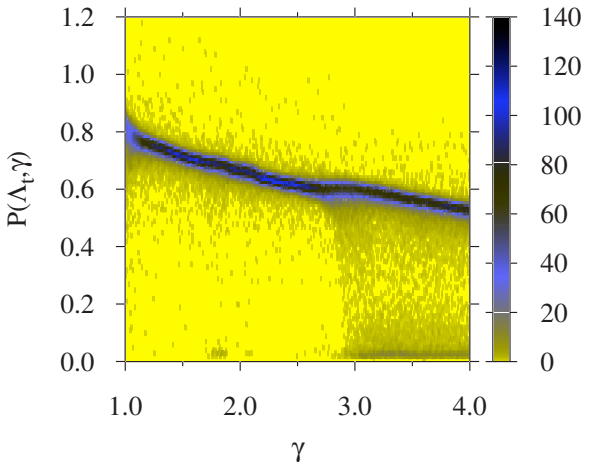

FIG. 3. (Color online) Finite-time distribution of the largest Lyapunov exponent $P(\Lambda_t, \gamma)$ calculated over 400 trajectories up to time $t=10^4$ and for $r_0=0.1$. With increasing $P(\Lambda_t, \gamma)$ the color changes from light to dark (white over yellow and blue to black).

$$\left.\frac{\partial P(\Lambda_t, \gamma)}{\partial \Lambda_t}\right|_{\Lambda_t=\Lambda_t^p} = 0. \tag{18}$$

For a mass ratio between $\gamma \sim 1.5$ and $\gamma \sim 2.2$, many initial condition lead to the same Λ_t. In this region, $\Lambda_t^p(\gamma)$ has a maximum as a function of γ. In other words, almost all initial conditions converge to the same LE and the dynamics should approach an "ergodiclike" motion. In fact, in this region the gray points (related to sticky or trapped trajectories) below the main curve almost disappear.

A similar behavior is found in the short interaction limit ($r_0=0.1$) shown in Fig. 3. Compared to Fig. 2, two main differences can be observed: first, the maximum for $\Lambda_t^p(\gamma)$ from Fig. 2 (between $\gamma \sim 1.5$ and $\gamma \sim 2.2$) is divided into two maxima, one close to 1.5 and the other one close to 2.4. Therefore, a minimum of $\Lambda_t^p(\gamma)$ appears in between ($\gamma \sim 1.9$), where trapped trajectories are expected to occur more often if compared with the two maxima $\gamma \sim 1.5$ and 2.4. Second, the abrupt appearance of many gray points below the main curve close to $\gamma \sim 2.7$, which may indicate that a regular island is born. This will be shown in more detail below.

A more systematic way to uncover this trend is to follow $P(\Lambda_t^p, \gamma) \equiv P_\Lambda(\gamma)$ as a function of the mass ratio γ shown in Fig. 4 (top). If P_Λ is large, a large fraction of initial conditions lead to the same Λ_t and trapped trajectories are rare. For example, the maximum of $P_\Lambda(\gamma)$ in Fig. 4 (top, $r_0 \to \infty$, black curve) close to $\gamma \sim 1.9$, is the region in Fig. 2 where gray points below the main curve are rare. The fast variation of $P_\Lambda(\gamma)$ is due to statistical fluctuations in the determination of Λ_t over the 400 initial conditions. However, two main valleys can be identified in the black curve of Fig. 4, one close to $\gamma=1$ and the other close to $\gamma=3$. These are exactly the mass ratios for which the hard-point like collision dynamics (Sec. II) is integrable. The gray curve of Fig. 4 for the short interaction ($r_0=0.1$), which is closer to the limit of hard-point collisions, presents an additional little valley at

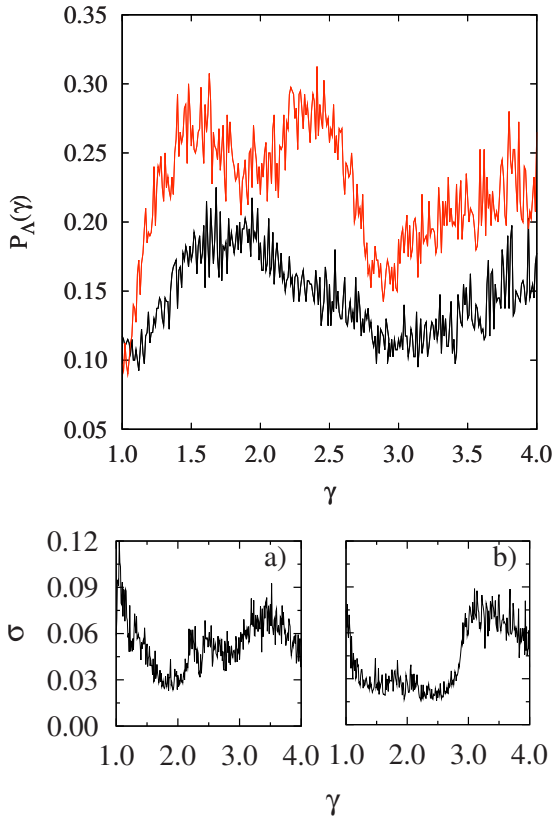

FIG. 4. (Color online) Top: normalized distribution $P_\Lambda(\gamma)$ of the most probable Lyapunov exponent Λ_t^p for $r_0 \to \infty$ (black) and $r_0=0.1$ (gray). Bottom: σ for (a) $r_0 \to \infty$ and (b) $r_0=0.1$.

$\gamma \sim 1.9$. This is the pseudointegrable case with genus $g=2$ which appears in the hard-point collision. In other words, if γ is close to values for which the dynamics in the pointlike gas is integrable ($g=1$) or "simpler" ($g=2$), then the dispersion around Λ_t^p increases so that $P_\Lambda(\gamma)$ decreases, and signatures of nonergodicity are expected under additional Yukawa interaction. Another interesting observation is that the minimum at $\gamma \sim 1.9$ (see gray curve from Fig. 4) disappears in the long interaction limit $r_0 \to \infty$ (see black curve from Fig. 4). It means that the regular motion from the integrable cases of the hard-point collision survives longer under the perturbation of the soft interaction than the regular motion from the pseudointegrable case.

For fully chaotic systems the quantity $P_\Lambda(\gamma)$ is just the maximum of a Gaussian distribution and it should increase linearly with t, since the variance $\sigma=(\langle\Lambda_t^2-\langle\Lambda_t\rangle^2\rangle)^{1/2}$ for such systems goes with $1/t$. This behavior of σ has been observed by studying ergodicity in high-dimensional sympletic maps [27] and used for the detection of small islands in the standard map [28]. For our case we found that the time dependence of $P_\Lambda(\gamma)$ goes with $\sim t^{0.3}$, which means that a significant number of islands is present. In order to compare σ with $P_\Lambda(\gamma)$, Figs. 4(a) and 4(b) show the behavior of σ as a function of γ. Each time trapped trajectories are present, σ should has a maximum, exactly the opposite behavior from $P_\Lambda(\gamma)$. In Fig. 4(a) we see two maxima, one close to $\gamma=1.0$, which corresponds to the minima of $P_\Lambda(\gamma)$ for the same value of γ, and the other one at $\gamma \sim 3.5$, which as no

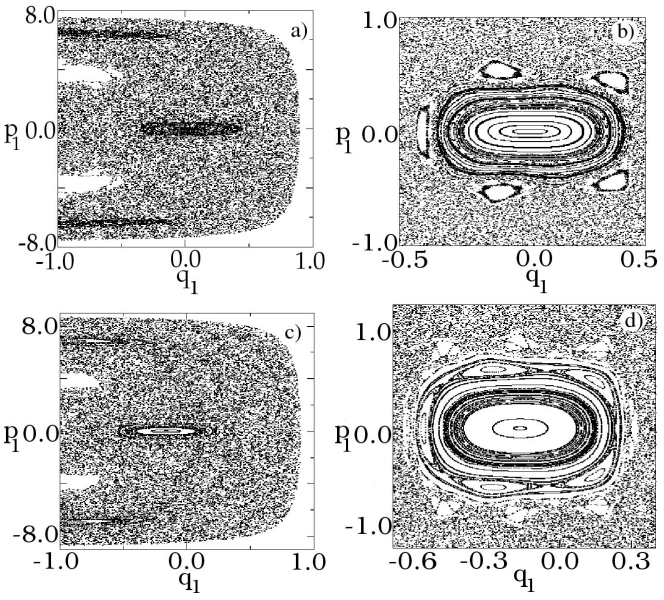

FIG. 5. Poincaré surfaces of section for $r_0 \to \infty$ and (a) $\gamma=3.0$ and (c) $\gamma=4.0$. (b) and (d) are the corresponding magnifications of the quasiregular regions.

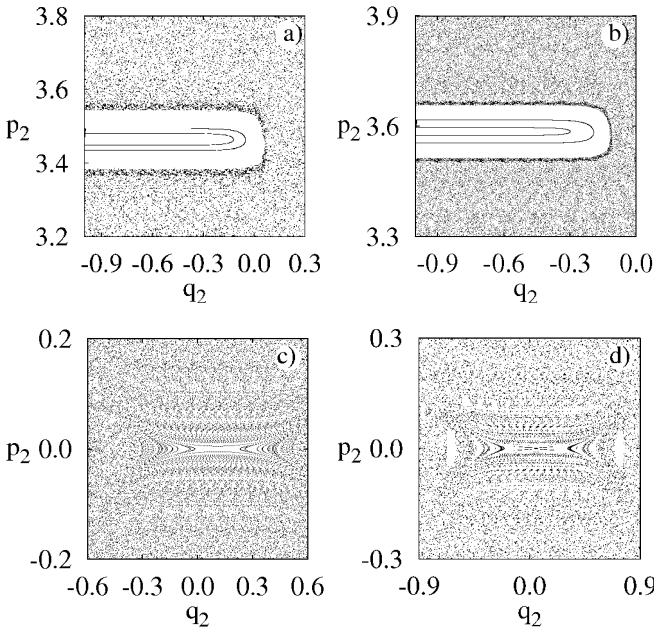

FIG. 6. Magnification of the Poincaré surfaces of section with $r_0=0.1$ for (a) $\gamma=1.5$, (b) $\gamma=1.8$, (c) $\gamma=2.6$, and (d) $\gamma=2.8$.

analog for $P_\Lambda(\gamma)$. For Fig. 4(b) we again see two maxima, one close to $\gamma=1.0$ and the other one located between $\gamma \sim 3.0$ and $\gamma \sim 3.5$. Besides the peaks at $\gamma=1.0$, the other peaks are not located at the integrable ($\gamma=3.0$) and pseudointegrable ($\gamma \sim 1.9$) cases from the hard-point like collisions cases. The peak around $\gamma \sim 3.0$ in Fig. 4(b) is correct, but by far not precise. This shows that the quantity σ is not sensible enough to detect signatures of the regular dynamics from the hard-point collision case. The reason for this is that σ is not able to detect small regular islands which appear in the phase space, such as, for example, the points related to zero LEs in Fig. 3 for $\gamma=1.9$. It is worth mentioning that the maxima and minima from $P_\Lambda(\gamma)$ do not change significantly with the number of initial conditions.

We can conclude that signatures from regular structures in phase space exist and are uncovered by the dispersion of the largest Lyapunov exponent Λ_t most clearly visible along the cut $P_\Lambda(\gamma)$ defined by the number of occurrences of the most probable Lyapunov exponent Λ_t^p [Eq. (18)]. No such signatures, however, are visible in less sensitive quantities such as the mean Lyapunov exponent $\langle \Lambda_t \rangle$ or the fluctuation σ.

The interpretation of the Lyapunov properties are supported by the relevant Poincaré surfaces of section (PSS). Figure 5 (top) shows PSS for interaction $r_0 \to \infty$ and cases $\gamma=3.0$ and $\gamma=4.0$, where $P_\Lambda(\gamma)$ has a minimum and maximum (see black curve in Fig. 4), respectively. Although the system is more chaotic for $\gamma=3.0$ than for $\gamma=4.0$, trapped trajectories appear near the island for $\gamma=3.0$ [see the corresponding magnification in Fig. 5 (top, right)]. Such trapped motion near regular islands, which does not appear for $\gamma=4.0$ [see Fig. 5 (bottom, right)], affects $P(\Lambda_t^p, \gamma)$ and, consequently, $P_\Lambda(\gamma)$ has a minimum near $\gamma=3.0$. Another example is shown in Fig. 6 for $r_0=0.1$. For $\gamma=1.5$ (top, left), which has a maximum in Fig. 4 (top, gray curve), no trapped trajectories are found up to the time propagated. For $\gamma=1.8$ (top, right), which has a minimum in Fig. 4 (top, gray curve), trapped trajectories start to appear. Moreover, the abrupt appearance of gray points for $\gamma \sim 2.7$ below the main curve of Fig. 3 can be nicely explained using the PSS. Figure 6 compares the PSS for $\gamma=2.6$ (bottom, left) with $\gamma=2.8$ (bottom, right), where gray points appear in Fig. 3. Clearly, it can be seen that when a regular island is born trapped trajectories start to appear around the island and, as a consequence, many initial conditions with lower LE are obtained (gray points in Fig. 4). The regular island is related to a period-4 orbit, which has the following property: for each second hit of particle 1 with the left wall, particle 2 is at rest. There is a similar periodic orbit for the hard-point collision case [20].

Note that although $P_\Lambda(\gamma)$ is determined only from trajectories with positive Λ_t, it provides information about the amount of regular structure in phase space through chaotic trajectories which are trapped close to regular islands. Since trapped trajectories are characteristic for mixing in phase space, $P_\Lambda(\gamma)$ provides a tool to analyze phase-space mixing.

IV. TWO PARTICLES IN A CIRCULAR BILLIARD WITH YUKAWA INTERACTION

In order to show the utility of $P_\Lambda(\gamma)$ for systems with higher dimensions, we discuss now the case of two interacting particles in a circular billiard. The interaction between particles is still of Yukawa type. The chaotic motion is now generated by the combined effect of the curvature of the walls from the circular billiard and the double collisions discussed in last section. The phase space is eight dimensional, and it is not possible to construct an adequate PSS which allows us to look at the underlying dynamics. Trajectories will fill out any chosen PSS, and no information about details of the dynamics can be obtained. Sticky trajectories, for ex-

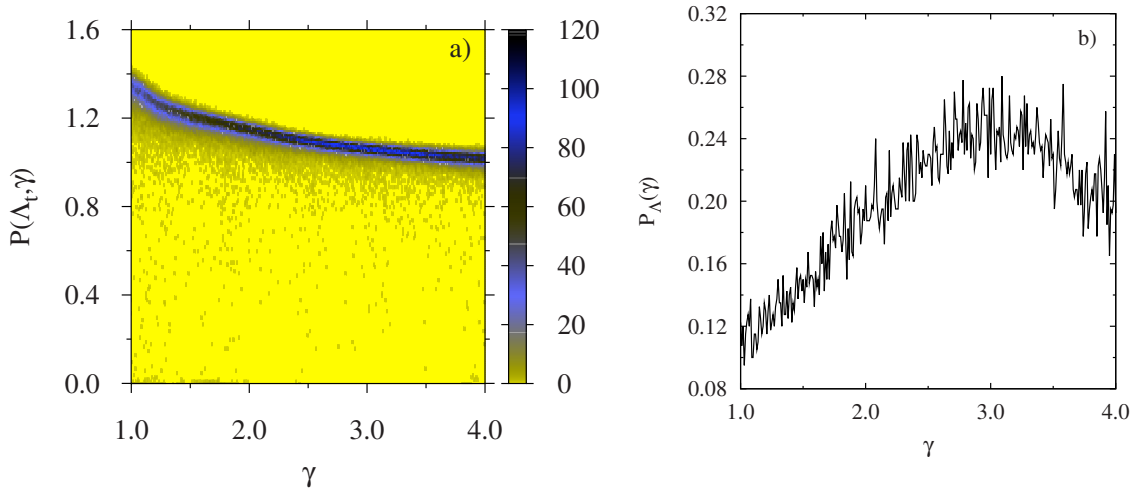

FIG. 7. (Color online) (a) Finite-time distribution of the largest Lyapunov exponent $P(\Lambda_t,\gamma)$ calculated over 400 trajectories up to time $t=10^4$ and for $r_0\to\infty$ for the circular billiard. With increasing $P(\Lambda_t,\gamma)$ the color changes from light to dark (white over yellow and blue to black). (b) Normalized distribution $P_\Lambda(\gamma)$ of the number of occurrences of the most probable Lyapunov exponent Λ_t^p.

ample, which may cause nonergodicity due to a partial focusing of trajectories [30], are difficult to detect. In such partial focusing, an infinitesimal family of nearby trajectories that starts out parallel will lead to Lyapunov exponents which converge very slowly in time. This is a typical behavior in high-dimensional quasiregular systems. In this section we show the effectiveness of $P_\Lambda(\gamma)$ to obtain relevant information in high-dimensional quasiregular systems.

Figure 7(a) shows the finite-time distribution of the largest LE for the case of long-range interaction ($r_0\to\infty$) in the circular billiard. The value of the mean LE calculated with the 400 initial conditions decreases by growing the mass ratio and the regular motion increases. This is the only information we can get from the LE about the complicated dynamics of the two interacting particles inside the billiard. However, the gray points below the main curve of Fig. 7(a) are related to chaotic trajectories which were trapped for a while close to regular islands. Therefore some additional information about sticky trajectories and the amount of quasiregular motion in phase space may be obtained from $P_\Lambda(\gamma)$. This is shown in Fig. 7(b). One minimum is observed close to $\gamma\sim 1.0$ where trapped trajectories and partial focusing of trajectories in phase space are expected. On the other hand, a more ergodiclike motion is expected for $\gamma\sim 3.0$, where $P_\Lambda(\gamma)$ has a maximum. This is different from the results for the 1D box from the last section (see the minimum for $r\to\infty$ at $\gamma=3.0$ in Fig. 4, top). In other words, we clearly see that signatures from the integrable case $\gamma=3.0$ from the 1D hard-point like collision case disappear in the two-dimensional case. This tells us that the dynamics from the integrable case $\gamma=3.0$ is a consequence of the fact that particles cannot pass each other in the 1D case. As the mass ratio increases to $\gamma=4.0$, the LE decreases and the system is more regular. In this case $P_\Lambda(\gamma)$ also decreases slowly and the amount of regular islands, and the motion around them, increases.

V. CONCLUSIONS

Usually, chaotic motion is generated through nonlinear equations of motion. As a consequence, exponential divergence of nearby trajectories occurs, which can be quantified by positive Lyapunov exponents. Another source of chaotic motion emerges even for linear equations of motion through boundary conditions. The advantage of such systems is the possibility to obtain rigorous mathematical results. One example is a point particle moving among high-dimensional cylindrical scatterers [29], which is similar to the high-dimensional Lorentz gas. In these systems, strongly chaotic motion is generated due to the convex curvature of hard disks or spheres. In fact, the collision time delay between nearby trajectories due to the curvature of the surface is responsible for the chaotic motion.

Curved boundaries are not present in the one-dimensional confinement considered in this paper. For the hard-point like collision case nonergodic motion is generated when the mass ratio gives a θ value [from Eq. (1)] which is a rational multiple of π. Ergodic motion, on the other hand, may be obtained for irrational multiples of θ/π. We have shown that for additional soft Yukawa interactions between the two particles, chaotic motion is obtained for any mass ratio. *Double* collisions of particles, which occur very close to the walls, are essential to generate positive LEs in the short-interaction-range limit. The collisional time delay in tangent space, together with the soft Yukawa interaction, is responsible for the chaotic motion. The mean of the largest finite-time LE, $\langle\Lambda_t\rangle$, decreases smoothly as the mass ratio increases and does not provide detailed information about the phase-space structure. This type of information is provided by the probability distribution of the largest finite-time Lyapunov exponent $P(\Lambda_t,\gamma)$. It reveals that the dispersion around $\langle\Lambda_t\rangle$ increases when trapped trajectories are present in the phase space. We have shown that a cut through $P(\Lambda_t,\gamma)$ along the number of occurrences of the most probable Lyapunov exponent $P_\Lambda(\gamma)$ gives a quantitative measure of the influence of regular motion in mixed phase space. Specifically for the system studied here, we have shown that $P_\Lambda(\gamma)$ decreases when the structure in phase space is more regular and the mass ratio is close to the integrable cases $\gamma=1,3$ (genus $g=1$) or to the "simpler" dynamics (pseudointegrable at $\gamma\sim 1.9$, with $g=2$)

from the hard-point like collision. We also observed that the regular motion of the integrable cases from the hard-point collision survives longer under perturbation of the soft interaction than regular motion from the pseudointegrable case. Hence, the dynamics under the additional Yukawa interaction, although in principle chaotic, "remembers" the integrable and pseudointegrable dynamics in the system without the soft Yukawa interaction. This is certainly a subtle effect and, therefore, we expect that in general the number of occurrences of the most probable Lyapunov exponent provides a sensitive tool to probe details in phase-space dynamics. We have also shown that this quantity is much more sensitive if compared with the mean-square fluctuations of the LE. In contrast to Poincaré sections this tool is easily applicable in higher-dimensional systems, where trapped trajectories may cause nonergodicity due to a partial focusing of trajectories [30]. In order to show this we calculated $P(\Lambda_t, \gamma)$ for two interacting particles in a circular billiard, where the phase space is eight dimensional and it is not possible to the construct an adequate Poincaré section to analyze the dynamics. We show that by increasing the mass ratio, the mean LE decreases and the system becomes more regular. Furthermore, for a minimum of $P_\Lambda(\gamma)$ at $\gamma \sim 1.0$ trapped trajectories are expected and for a maximum at $\gamma \sim 3.0$ ergodiclike motion is expected. Therefore, $P_\Lambda(\gamma)$ can be used in higher-dimensional systems as a tool to characterize the dynamics.

ACKNOWLEDGMENTS

C.M. thanks CAPES and M.W.B. thanks CNPq for financial support. M.W.B. is grateful to M. G. E. da Luz, J. D. Szezech, A. S. de Wijn, and S. Tomsovic for helpful discussions.

[1] Ya. G. Sinai, Funct. Anal. Appl. **2**, 61 (1968).
[2] L. A. Bunimovich, Funct. Anal. Appl. **8**, 254 (1974).
[3] O. Bohigas, D. Boosé, R. E. de Carvalho, and V. Marvulle, Nucl. Phys. A. **560**, 197 (1993).
[4] M. A. Reed and W. P. Kirk, *Nanostructure and Fabrication* (Academic, Boston, 1989).
[5] O. Gunawan, Y. P. Shkolnikov, E. P. De Poortere, E. Tutuc, and M. Shayegan, Phys. Rev. Lett. **93**, 246603 (2004); U. Merkt, J. Huser, and M. Wagner, Phys. Rev. B **43**, 7320 (1991).
[6] L. Meza-Montes and S. E. Ulloa, Phys. Rev. E **55**, R6319 (1997).
[7] L. Meza-Montes, F. M. Izrailev, and S. E. Ulloa, Phys. Status Solidi B **220**, 721 (2000); L. Meza-Montes and S. E. Ulloa, Physica B (Amsterdam) **249-251**, 224 (1998).
[8] G. Casati and J. Ford, J. Comput. Phys. **20**, 97 (1976).
[9] P. Cipriani, S. Denisov, and A. Politi, Phys. Rev. Lett. **94**, 244301 (2005); P. Grassberger, W. Nadler, and L. Yang, *ibid.* **89**, 180601 (2002).
[10] G. Casati, C. Tsallis, and F. Baldovin, Europhys. Lett. **72**, 355 (2005).
[11] F. Cecconi, D. del-Castillo-Negrete, M. Falcioni, and A. Vulpiani, Physica D **180**, 129 (2003).
[12] G. M. Zaslavsky and M. Edelman, Phys. Rev. E **72**, 036204 (2005); E. G. Altmann, A. Motter, and H. Kantz, Chaos **15**, 033105 (2005); G. M. Zaslavsky, Phys. Rep. **371**, 461 (2002).
[13] S. L. Glashow and L. Mittag, J. Stat. Phys. **87**, 937 (1997); S. G. Cox and G. J. Ackland, Phys. Rev. Lett. **84**, 2362 (2000).
[14] G. Casati and T. Prosen, Phys. Rev. Lett. **83**, 4729 (1999).
[15] P. Kornfeld, S. V. Fomin, and Y. G. Sinai, *Ergodic Theory* (Springer, Berlin, 1982); J. Walker, *The Flying Circus of Physics* (Wiley, New York, 1977); S. Redner, Am. J. Phys. **72**, 1492 (2004).
[16] V. I. Arnold and A. Avez, *Ergodic Problems of Classical Mechanics* (Benjamin, New York, 1968).
[17] M. Van Vessen, Jr., M. C. Santos, Bin Kang Cheng, and M. G. E. da Luz, Phys. Rev. E **64**, 026201 (2001); A. G. Miltenburg and Th. W. Ruijgrok, Physica A **210**, 476 (1994); V. V. Koslov and D. V. Treshchnev, *Billiards: A Genetic Introduction to the Dynamics of Systems with Impacts* (American Mathematical Society, Providence, RI, 1991).
[18] T. Gorin, J. Math. Phys. **34**, 8281 (2001).
[19] A. Shudo and Y. Shimizu, Phys. Rev. E **47**, 54 (1993).
[20] E. Gutkin, J. Stat. Phys. **83**, 7 (1996).
[21] P. J. Richens and M. V. Berry, Physica D **2**, 495 (1981).
[22] A. Azevedo, M. W. Beims, and M. G. E. da Luz (unpublished).
[23] G. Boffetta, M. Cencini, M. Falcioni, and A. Vulpiani, Phys. Rep. **356**, 367 (2002).
[24] Ch. Dellago, H. A. Posch, and W. G. Hoover, Phys. Rev. E **53**, 1485 (1996); Ch. Dellago and H. A. Posch, *ibid.* **52**, 2401 (1995).
[25] A. Crisanti, G. Paladin, and A. Vulpiani, *Products of Random Matrices in Statistical Physics* (Springer-Verlag, Heidelberg, 1993); M. A. Sepúlveda, R. Badii, and E. Pollak, Phys. Rev. Lett. **63**, 1226 (1989).
[26] P. Grassberger, R. Badii, and A. Politi, J. Stat. Phys. **51**, 135 (1988); E. J. Kostelich, I. Kan, C. Grebogi, E. Ott, and J. A. Yorke, Physica D **109**, 81 (1997); H. Schomerus and M. Titov, Phys. Rev. E **66**, 066207 (2002); F. Feudel, A. Witt, M. Gellert, J. Kurths, C. Grebori, and M. A. F. Sanjuán, Chaos Solitons Fractals **24**, 947 (2005).
[27] M. Falcioni, U. M. B. Marconi, and A. Vulpiani, Phys. Rev. A **44**, 2263 (1991).
[28] S. Tomsovic and A. Lakshminarayan, Phys. Rev. E **76**, 036207 (2007).
[29] A. S. de Wijn and H. van Beijeren, Phys. Rev. E **70**, 016207 (2004); A. S. de Wijn, Ph.D. thesis, Instituut voor Theoretische Fysica, Leuven, The Netherlands, 2004.
[30] V. J. Donnay, J. Stat. Phys. **96**, 1021 (1999).